0031-3998/07/6202-0156
PEDIATRIC RESEARCH
Vol. 62, No. 2, 2007
Printed in U.S.A.

The Ocular Anomalies in a Cystinosis Animal Model Mimic Disease Pathogenesis

VASILIKI KALATZIS, NICOLAS SERRATRICE, CLAIRE HIPPERT, OLIVIER PAYET, CARL ARNDT, CHANTAL CAZEVIEILLE, TANGUI MAURICE, CHRISTIAN HAMEL, FRANÇOIS MALECAZE, CORINNE ANTIGNAC, AGNES MÜLLER, AND ERIC J. KREMER

Institut de Génétique Moléculaire de Montpellier [V.K., N.S., C.H., E.J.K.]; UMR 5535 CNRS-Universités Montpellier I&II [V.K., N.S., C.H., E.J.K.], 34293 Montpellier, France; Inserm U583 [O.P., C.Arndt, C.C., C.H., A.M.], Institut des Neurosciences de Montpellier, Hôpital St. Eloi, 34091 Montpellier, France; Inserm U710 [T.M.], 34095 Montpellier, France; EPHE [T.M.], 75017 Paris, France; Université de Montpellier II [T.M.], 34095 Montpellier, France; Inserm U563 [F.M.]; Département d'Ophtalmologie [F.M.], Hôpital Purpan, 31059 Toulouse, France; Inserm U574 [C.Antignac], 75015 Paris, France; UMRS574 [C.A.], Faculté de Médecine René Descartes, Université Paris Descartes, 75015 Paris, France

ABSTRACT: Cystinosis is a lysosomal storage disorder characterized by abnormal accumulation of cystine, which forms crystals at high concentrations. The causative gene *CTNS* encodes cystinosin, the lysosomal cystine transporter. The eye is one of the first organs affected (corneal lesions and photophobia in the first and visual impairment in the second decade of life). We characterized the ocular anomalies of $Ctns^{-/-}$ mice to determine whether they mimic those of patients. The most dramatic cystine accumulation was seen in the iris, ciliary body, and cornea of $Ctns^{-/-}$ mice. Consistently, $Ctns^{-/-}$ mice had a low intraocular pressure (IOP) and seemed mildly photophobic. Retinal cystine levels were elevated but increased less dramatically with age. Consistently, the retina was intact and electroretinogram (ERG) profiles were normal in mice younger than 19 mo; beyond this age, retinal crystals and lesions appeared. Finally, the lens contained the lowest cystine levels and crystals were not seen. The temporospatial pattern of cystine accumulation in $Ctns^{-/-}$ mice parallels that of patients and validates the mice as a model for the ocular anomalies of cystinosis. This work is a prerequisite step to the testing of novel ocular cystine-depleting therapies. **(*Pediatr Res* 62: 156–162, 2007)**

In most cases, abnormal lysosomal storage is the consequence of defects in lysosomal hydrolases, which lead to the accumulation of nonmetabolized macromolecules. However, abnormal storage of digestion by-products can also result from defects in lysosomal transporters. The clinical manifestations of abnormal storage give rise to a heterogeneous group of multisystemic diseases termed lysosomal storage diseases (LSDs).

An accumulation of lysosomal cystine, which forms crystals at high concentrations, gives rise to the autosomal recessive disorder cystinosis (1). Patients are generally grouped into three clinical forms based on the age at onset and severity of the symptoms. The most severe and common form, infantile cystinosis, generally appears between 6 and 12 mo with the renal Fanconi syndrome and can proceed to end-stage renal disease (ESRD) by 10 y. Corneal cystine crystals appear from the first year of life. The resulting anomalies, including photophobia, blepharospasm, and lesions, appear from 3 to 4 y (2,3) and lead to varying degrees of visual discomfort and impairment in the first or second decade (4). After renal transplantation, continuous widespread cystine accumulation leads to multisystemic anomalies. Notably, retinal depigmentation appears by 7 y and can evolve into blindness between 13 and 40 y in 15% of cases (5). Juvenile cystinosis appears during adolescence with photophobia and renal impairment, but not necessarily Fanconi syndrome; progression to ESRD is much slower. Finally, ocular cystinosis is characterized by corneal crystals, with or without photophobia, and absence of renal dysfunction.

Lysosomal cystine storage is due to defects in the cystine transporter cystinosin (6), encoded by the gene *CTNS* (7). A functional assay of nontruncating *CTNS* mutations showed that the level of cystine transport inhibition correlates with severity of symptoms (8). Generally, transport is abolished in infantile cystinosis, whereas residual activity (9%–20%) gives rise to the juvenile and ocular forms.

Mixed background *Ctns* knockout ($Ctns^{-/-}$) mice were generated and partially characterized (9). Despite high renal cystine levels, $Ctns^{-/-}$ mice showed no evidence of renal dysfunction or failure. However, preliminary studies suggested the presence of ocular anomalies. In this study, we generated pure background $Ctns^{-/-}$ mice and characterized the ocular anomalies using a threefold approach. First, we quantified the cystine content of different tissues as a function of age. Second, we correlated these data with the histologic detection of cystine crystals. Finally, we used clinical tests to evaluate the biologic effect of cystine accumulation. Together, this work provides a temporal and spatial guide of the ocular anomalies in the $Ctns^{-/-}$ mice and validates these animals as a model for the ocular anomalies of cystinosis.

Received November 28, 2006; accepted March 7, 2007.

Correspondence: Vasiliki Kalatzis, Ph.D., IGMM CNRS UMR 5535, 1919 Route de Mende, 34293 Montpellier, France; e-mail: vasiliki.kalatzis@igmm.cnrs.fr.

V.K. and E.J.K. are Inserm scientists. N.S. and C.H. are Vaincre les Maladies Lysosomales (France) and Cystinosis Research Network (Lake Forest, IL) fellows, respectively.

This project was funded by the Association Française contre les Myopathies (France) and the Cystinosis Research Network.

Abbreviations: ERG, electroretinogram; **IOP,** intraocular pressure; **RPE,** retinal pigment epithelium; **TEM,** transmission electron microscopy

METHODS

Animals. Male 129Sv-C57BL/6 *Ctns*$^{+/+}$ and *Ctns*$^{-/-}$ mice (9) were back-crossed with wild-type C57BL/6 females for eight generations (CDTA, Orleans, France). Housing and expansion were continued at the IGMM according to the European Communities Council Directive 86/609/EEC. Age-matched mice were used for the experiments.

Dissection of ocular tissues. Mouse eyes were enucleated from euthanized mice, and the anterior and posterior segments were separated by a circumferential incision at the corneoscleral junction. The cornea and iris (containing the ciliary body) were separated. The lens was removed from the posterior cup, and the neural retina was separated from the underlying RPE. After removal, we observed an irregular mosaic appearance of the underlying pigmented tissues in *Ctns*$^{-/-}$ mice 11 mo and older. Due to technical limitations, we did not collect the RPE, pigmented choroid, and sclera. Furthermore, beyond 13 mo, the iris had degenerated and adhered to the cornea and could not be collected.

Assay of cystine levels. The equivalent tissues from each eye were pooled and homogenized in 0.65 mg/mL *N*-ethylmaleimide. After sonication, the proteins were precipitated using 3% sulfosalicylic acid and removed by centrifugation. The protein pellet was dissolved in 0.1 N NaOH and quantified using the BCA protein assay kit (Pierce-Perbio Science, France). The protein-depleted supernatant was assayed for cystine content by radiocompetition with ^{14}C-cystine (Perkin-Elmer Life Sciences, France) for the cystine binding protein (CBP) (Riverside Scientific Enterprises, Bainbridge Island, WA) (10). After filtration, the ^{14}C-cystine–CBP complex was measured by liquid scintillation (Formula 989; Perkin Elmer).

Light microscopy. Enucleated eyes were fixed in 4% paraformaldehyde and embedded in paraffin. Unstained sagittal 2.5 μm-thick sections were screened for crystals using a Leica DMRA microscope.

TEM. Enucleated eyes were fixed in 3.3% glutaraldehyde, postfixed in 2% osmium tetraoxide, and embedded in epoxy resin. Frontal and sagittal 1 μm-thick sections were stained with toluidine blue and observed under light microscopy. Frontal and sagittal 85 nm-thick sections were stained with uranyl acetate and lead citrate and visualized by TEM (Hitachi H7100).

Clinical examinations. Mice were tested under general anesthesia [10 mg/kg xylazine (Bayer Pharma, France) and 100 mg/kg ketamine (Merial, France)]. Eyes were dilated with 0.5% tropicamide (MSD-Chibret, Paris, France) and anesthetized locally with 0.4% oxybuprocaine hydrochloride (MSD-Chibret).

Slit-lamp photography. Images of the cornea and iris were taken using the IMAGEnet imaging system (Topcon, Tokyo) comprising a photographic slit lamp (SL-D7) and digital camera (DC-1).

IOP. The IOP of mice 15 mo and older (six per genotype) was measured using a Tonopen XL (Medtronic Solan) (11). The median of 20 measures with an error $\leq$5% (10 per eye) was used as the experimental value for each mouse. The final IOP of each genotype is expressed as the median (Q1; Q3) of the six values.

ERGs. After 12-h dark adaptation, the bilateral ERG responses to seven white-light flashes (frequency of 1 Hz and luminance of 6 cd/m^2) were recorded using platinum corneal electrodes and a VisioSystem (SIEM BIO-Médicale, France). The amplitude values for each eye were averaged per mouse.

Behavioral test. Photophobia was assayed in mice 17 mo and older (10 per genotype) using a light/dark exploration box (12). Each mouse was placed in the dark compartment, and exploratory activity was videotaped for 10 min. The total time spent in and the number of entries into the light compartment, the mean duration of each visit, and the number of visits with a duration time $<$10 s were recorded.

Statistical analysis. For the behavioral test, statistical analyses were performed using an unpaired *t* test. For the remaining studies, due to the small sample sizes, data were analyzed using nonparametric statistical tests: Mann-Whitney (two groups of data) or Kruskal-Wallis (more than two groups of data) followed by a Siegel-Castellan 2 $\times$ 2 comparison (13).

RESULTS

Cystine levels. We detected elevated cystine levels in the iris (and ciliary body) of *Ctns*$^{-/-}$ mice compared with controls from 1 mo (sevenfold), in the cornea (ninefold) and retina (12-fold) from 3 mo, and in the lens (fivefold) from 7 mo (Fig. 1*A–D*). Among *Ctns*$^{-/-}$ tissues (Fig. 1*E*), cystine levels in the cornea and iris were the highest and increased at the greatest rate. Levels increased dramatically between 5 and 7 mo and peaked at 9 mo (62- and 145-fold for the cornea and iris, respectively). At 11 mo, we observed a decrease that was significantly different from the values at 9 or 13 mo for the iris ($p < 0.05$) but not for the cornea ($p > 0.05$). The corneal values remained stable beyond 13 mo (58-fold over wild type).

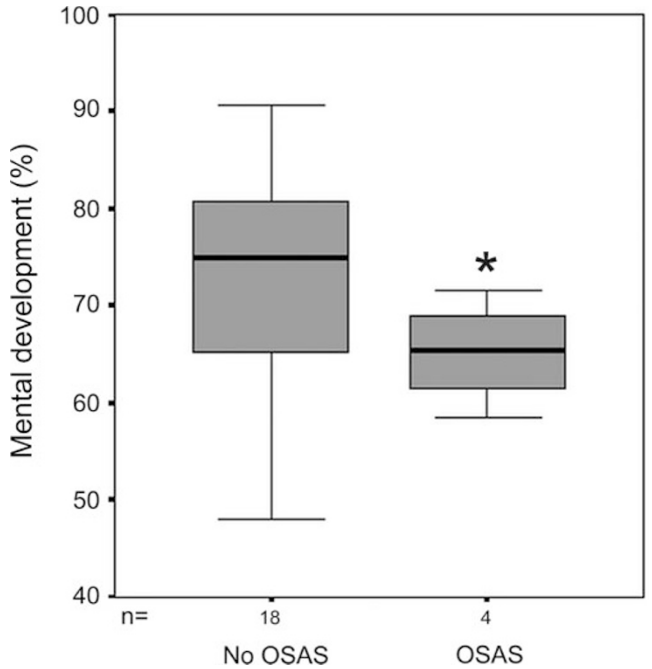

Figure 1. Cystine levels *vs* age. Levels in the iris (*A*), cornea, (*B*), retina (*C*), and lens (*D*). For *Ctns*$^{-/-}$ values (■), each point represents one mouse (– mean). For *Ctns*$^{+/+}$ values (◇), one representative mouse is shown. (*E*) Evolution of cystine accumulation (mean ± SEM, $n \geq 3$) in *Ctns*$^{-/-}$ mice. Wild-type levels were stable: 1.59 ± 0.18 (cornea), 0.62 ± 0.06 (iris), 0.33 ± 0.03 (retina), and 0.05 ± 0.01 (lens).

We observed a less dramatic increase in retinal levels with age: 60-fold over wild type at 9 mo. We also detected a decrease at 11 mo, which was significantly different from that at 9 mo ($p < 0.05$). Finally, the lens contained the lowest increase in cystine levels: sixfold over wild type at 9 mo, reaching 27-fold at 23 mo.

Cystine crystals and histologic lesions.

Iris. We detected rare crystals (Fig. 2*A–C*) from 1 mo that became abundant from 7 mo. Crystals were first distributed throughout the iris stroma and appeared in the pigmentary epithelium from 9 mo. The densest crystal concentration was at the iris–ciliary body junction. Their frequency decreased closer to the pupillary border. Moreover, in 19- and 22-mo-old *Ctns*$^{-/-}$ mice, we observed a fusion of the iris and cornea (Fig. 3*C* and *D*), consistent with the difficulties we encountered in collecting the iris during dissection.

Ciliary body. Similarly, we detected crystals in the ciliary body (Fig. 2*D–F*) from 1 mo, but these were larger and more abundant than those in the iris. Their size and number also increased with age, and they became strikingly abundant from 7 mo. Crystals were mainly located in the ciliary body stroma and appeared in the pigmented epithelium of the processes from 11 mo. We could not unambiguously find crystals in the nonpigmented epithelium.

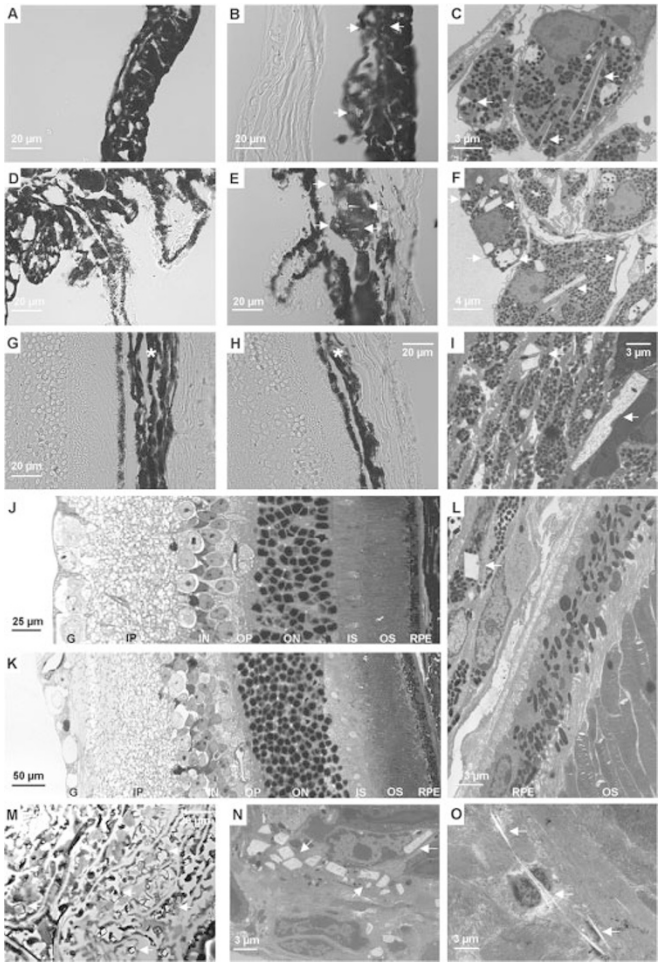

Figure 2. Cystine crystals (*arrows*) and lesions in young mice. (*A*) Iris of a 7-mo-old wild-type mouse. Crystals in the iris stroma of 11-mo-old (*B*) and 9-mo-old (*C*) *Ctns*$^{-/-}$ mice (TEM). (*D*) Ciliary body and processes of a 7-mo-old wild-type mouse. Abundant crystals in the ciliary body stroma of a 9-mo-old *Ctns*$^{-/-}$ mouse by light microscopy (*E*) and TEM (*F*). (*G*) Choroid (*) of an 11-mo-old wild-type mouse. (*H*) Degenerating choroid (*) of an 11-mo-old *Ctns*$^{-/-}$ mouse. (*I*) Crystals in the choroid of a 9-mo-old *Ctns*$^{-/-}$ mouse (TEM). Retinas of a 9-mo-old wild-type (*J*) and *Ctns*$^{-/-}$ (*K*) mouse (G, ganglion layer; IP, inner plexiform layer; IN, inner nuclear layer; OP, outer plexiform layer; ON, outer nuclear layer; IS, inner segments of photoreceptor cells; OS, outer segments). (*L*) Crystals in the choroid of a 9-mo-old *Ctns*$^{-/-}$ mouse (TEM). (*M*) Abundant rectangular crystals in the cornea of a 9-mo-old *Ctns*$^{-/-}$ mouse, and rectangular (*N*) and needle-shaped (*O*) crystals in the stromal keratocytes (TEM).

Choroid and sclera. We observed rare cystine crystals throughout the choroid (Fig. 2*G–I*) at 1 mo. These became abundant from 7 mo (Fig. 3*G* and *I*). Concomitantly, we observed that the *Ctns*$^{-/-}$ choroid was thinner and less homogeneous (Fig. 2*H*) than that of controls (Fig. 2*G*). The choroid continued to degenerate (Fig. 3*G*) and was almost nonexistent by 22 mo (Fig. 3*H*). Choroidal degeneration is consistent with the mosaic appearance of the pigmented tissues observed during dissection. Crystals became visible in the sclera from 3 mo (not shown). Initially, these were seen mainly in the posterior region clustered around the capillaries; however, from 9 mo, they were scattered throughout.

Lens and retina. We did not detect crystals in the lens, regardless of age. Up to 15 mo, we could not detect crystals in the retina. Furthermore, the neural retina and the RPE retained a homogeneous structure (Fig. 2*J–L*), suggesting the RPE did not contribute to the aforementioned mosaicism. Conversely, in 19- and 22-mo-old *Ctns*$^{-/-}$ mice, the RPE had degenerated (Fig. 3*H*, *K*, and *L*). Moreover, the photoreceptor segments and nuclei were absent and the inner nuclear layer constituted the most posterior layer of the neural retina and contained rare crystals (Fig. 3*L* and *M*).

Cornea. We could not detect cystine crystals in 2.5 μm-thick sections of the cornea. However, we observed abundant rectangular crystals in 1 μm-thick sections (Fig. 2*M*), suggesting the thicker sections masked the smaller (2–3 μm) crystals. Using 85 nm-thick sections (Fig. 2*N* and *O*), we also detected needle-shaped ($\leq 0.3 \times 10$ μm) crystals (Fig. 2*O*). In contrast to the iris and ciliary body, we did not detect corneal crystals at 1 mo. The crystals were located within the keratocytes throughout the stroma. We did not detect crystals in the epithelium, Bowman's layer (Fig. 3*C*), Descemet's membrane (Fig. 3*D*), or endothelium, regardless of age. Finally, in addition to anterior synechiae, we observed a vascularization of the cornea from 19 mo (Fig. 3*E*).

Taken together, the appearance of crystals is consistent with the cystine levels assayed: (1) absence of crystals in the lens, consistent with low cystine levels (2 nmol half cystine/mg protein maximum); (2) rare crystals in the retina of older mice when levels reached 30 nmol half cystine/mg protein, and (3) crystals in the iris and ciliary body before 5 mo, which became abundant from 7 mo, concomitant with the increase from 30–80 nmol half cystine/mg protein.

Clinical Examinations

Slit-lamp photography. We complemented our histologic studies with slit-lamp photography to compare the evolution of crystals in the cornea and iris. In both tissues, rare crystals were first seen at 3 mo (not shown). Crystals were evident but not abundant at 5 mo (Fig. 4*A* and *B*). However, from 7 (Fig. 4*C* and *D*) to 13 mo (Fig. 4*E* and *F*), crystals were abundant and easily detectable. Corneal crystals were fine and needle shaped, whereas those in the iris were denser, more square shaped, and highly visible.

Taken together, although corneal crystals appeared slightly later, their evolution paralleled that of the iris, consistent with the overlapping profile of cystine levels in these tissues.

IOP measures. IOP variations can be due to obstructed flow of aqueous humor (increased) or defective production by the ciliary body (decreased). Thus, we indirectly examined the effect of ciliary body crystals on humor production by measuring IOP. We recorded an IOP of 13 mm Hg (11.4; 13) in the wild-type C57BL/6 mice, consistent with that reported (12–14 mm Hg) (14). In contrast, the *Ctns*$^{-/-}$ mice had a lower IOP of 9 mm Hg (6.1; 9.4) ($p < 0.1$).

These results suggest that the crystals in the ciliary body of the *Ctns*$^{-/-}$ mice might disrupt aqueous humor production and account for the relative IOP decrease.

ERG profiles. We observed a classic ERG profile (negative "a" and positive "b" wave) for each genotype (Fig. 5*A*). We did not find a significant difference in a-wave amplitude with age in *Ctns*$^{+/+}$ ($p > 0.05$) or *Ctns*$^{-/-}$ ($p > 0.05$) mice (Fig. 5*B*). Similarly, we did not detect a difference in a-wave ampli-

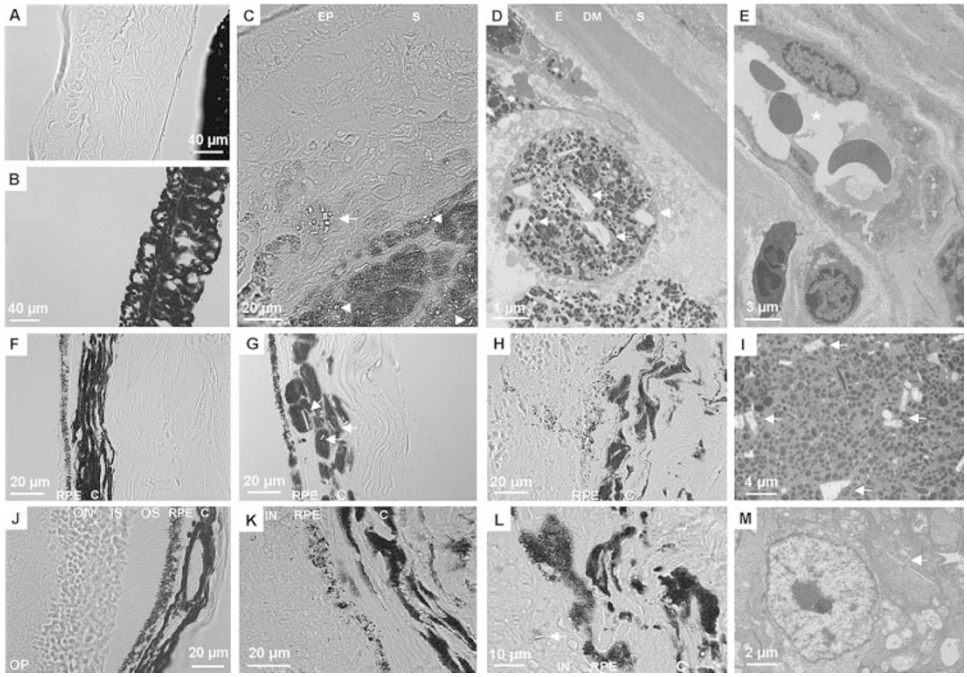

Figure 3. Cystine crystals (*arrows*) and lesions in older mice. Cornea (*A*) and iris (*B*) of a 19-mo-old wild-type mouse. (*C*) Anterior synechiae in a 22-mo-old *Ctns*$^{-/-}$ mouse with crystals in the cornea (S) and iris stroma (*arrowheads*; EP, epithelium). (*D*) Anterior synechiae in a 19-mo-old *Ctns*$^{-/-}$ mouse (TEM). The iris stroma, containing crystals, has adhered to the corneal endothelium (E) (DM, Descemet's membrane). (*E*) Corneal vascularization (*) in a 22-mo-old *Ctns*$^{-/-}$ mouse. (*F*) RPE and choroid (C) of a 19-mo-old wild-type mouse. (*G*) Intact RPE and degenerating choroid of a 15-mo-old *Ctns*$^{-/-}$ mouse. (*H*) Degenerated RPE and choroid of a 22-mo-old *Ctns*$^{-/-}$ mouse. (*I*) Crystals in the choroid of a 22-mo-old *Ctns*$^{-/-}$ mouse (TEM). (*J*) Retina of a 19-mo-old wild-type mouse. (*K*) Retina of a 22-mo-old *Ctns*$^{-/-}$ mouse showing a degenerated RPE and absent photoreceptor segments and nuclei. Crystals in the inner nuclear layer of 19-mo-old (*L*) and 22-mo-old (*M*) *Ctns*$^{-/-}$ retinas (TEM).

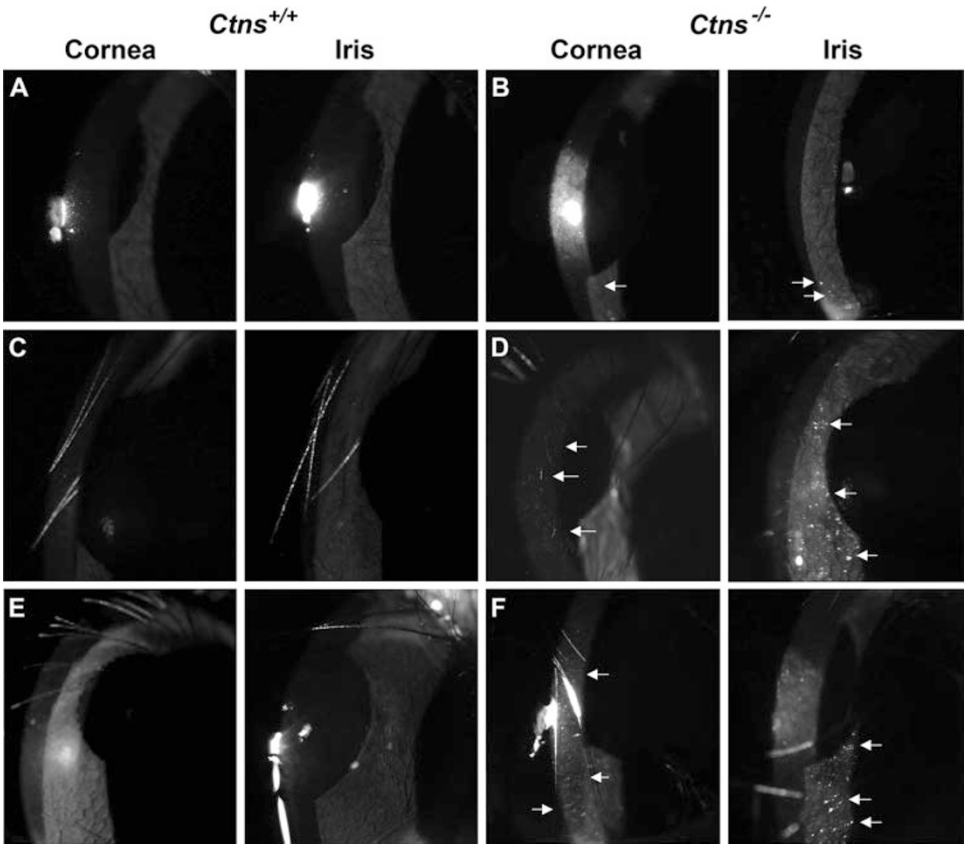

Figure 4. Slit-lamp photography. Crystal evolution (*arrows*) in the cornea and iris of *Ctns*$^{+/+}$ (*A*, *C*, and *E*) and *Ctns*$^{-/-}$ (*B*, *D*, and *F*) mice aged 5 (*A* and *B*), 7 (*C* and *D*), and 13 mo (*E* and *F*).

tude between the *Ctns*$^{+/+}$ and *Ctns*$^{-/-}$ response at any age ($p > 0.05$). Conversely, a significant decrease was seen in b-wave amplitude with age in *Ctns*$^{+/+}$ mice ($p < 0.05$), suggesting an age-related decrease in retinal function ($p < 0.05$ between 3 and 11 mo) (Fig. 5*C*). We also saw a nonsignificant decrease in *Ctns*$^{-/-}$ mice ($p > 0.05$). Last, we did not detect a significant difference in b-wave amplitude between the *Ctns*$^{+/+}$ and *Ctns*$^{-/-}$ response at any age ($p > 0.05$).

Taken together, these data suggest that retinal function was preserved in ≤11-mo-old *Ctns*$^{-/-}$ mice, consistent with the low retinal cystine levels and absence of crystals.

Light/dark exploration test. Both genotypes exhibited a clear preference for the dark compartment. However, the *Ctns*$^{-/-}$ mice showed an increase in the total time spent in the light compartment (Fig. 6*A*), but not in the number of entries or the mean duration of each visit (Fig. 6*B* and *C*). This

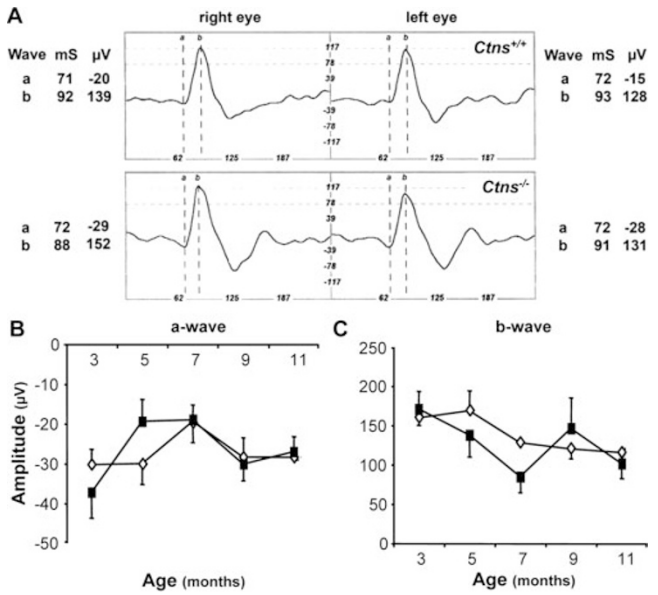

Figure 5. ERG studies of $Ctns^{+/+}$ and $Ctns^{-/-}$ mice. (*A*) ERG profiles of 7-mo-old mice. Evolution of the a wave (*B*) and b wave (measured from the a-wave trough to the b-wave peak) (*C*) responses (mean ± SEM, $n = 4$; ◇ $Ctns^{+/+}$, ■ $Ctns^{-/-}$).

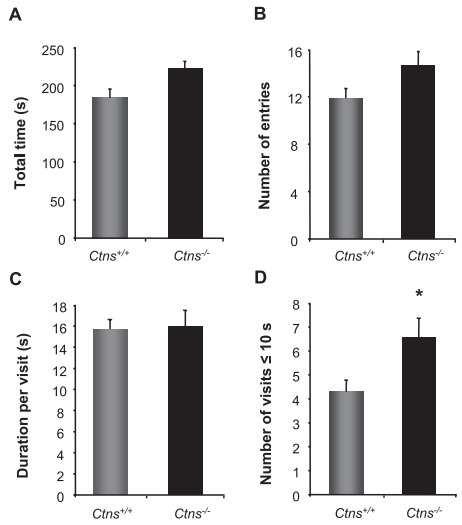

Figure 6. Light/dark exploration test. Total time spent in (*A*) and number of entries into (*B*) the light compartment, exploratory duration per visit (*C*), and number of visits with a duration ≤10 s (*D*). $*p < 0.05$.

difference was due to an increased number of short-duration (≤10 s) visits of 5.1 ± 0.3 s on average (Fig. 6*D*).

Although a classic photophobic behavior was not detected, our results highlight a need for the $Ctns^{-/-}$ mice to rapidly re-enter the dark compartment more often than controls.

DISCUSSION

Cystinosis is characterized by a tissue-variable lysosomal accumulation of cystine. We report here a biochemical, histologic, and clinical analysis of the ocular anomalies in C57BL/6 $Ctns^{-/-}$ mice as a function of age and discuss these anomalies in comparison with those of cystinosis patients.

Iris and ciliary body. Aside from the cornea, the cystine levels in human or murine ocular tissues have not been quantified previously. The iris (and ciliary body) of $Ctns^{-/-}$ mice showed the highest levels and fastest rate of cystine accumulation. The dramatic increase in levels between 5 and 7 mo, and thereafter remaining stable, pinpoints the period of lysosomal overloading. The dip in levels at 11 mo, although statistically significant, is likely due to the lower cystine levels, and low variation, in the four 11-mo-old $Ctns^{-/-}$ mice studied rather than having a physiologic significance.

Crystals were most abundant in the stroma of the ciliary body and, later, in the pigment epithelium of the processes. Although not highly significant, we also observed a lower IOP in $Ctns^{-/-}$ mice, suggesting that these crystals might interfere with aqueous humor production. We noted that the eyes of older $Ctns^{-/-}$ mice were smaller than those of controls, which is also consistent with a decreased IOP. Due to the continuity of the ciliary body and iris, we observed a similar temporospatial distribution of iris crystals, although they were less abundant. Furthermore, we demonstrated that the evolution of iris crystals can be followed by noninvasive slit-lamp photography. However, crystal detection from 3 mo suggests a limited sensitivity.

Similarly, in cystinosis patients, abundant crystals have been described in the ciliary body and less so in the iris (2,3,15–17). In the ciliary body, crystals were reported in the stroma and in the pigmented and nonpigmented epithelium. In the iris, crystals were reported throughout the stroma and in the pigment epithelium (3,16,17), and their presence was confirmed by biomicroscopic investigations (18,19). However, the biologic effects of cystine accumulation varied. To our knowledge, decreased IOP has not been reported in patients. In contrast crystal deposition, leading to a thickening and stiffening of the iris and consequently pupillary block, was reported to be responsible for angle-closure glaucoma (17). Furthermore, glaucoma-independent cases of pupillary block associated with posterior synechiae were also reported (18). The anterior synechiae that we observed in the $Ctns^{-/-}$ mice has not been reported in patients.

Cornea. The corneal cystine level and accumulation profile of $Ctns^{-/-}$ mice mirrors that of the iris. Corneal levels of a 12-y-old with infantile cystinosis (12.6 nmol half cystine/mg protein) (20) and in cultured stromal cells of a 59-y-old with mild ocular cystinosis (0.98 nmol half cystine/mg protein) (21) have been reported. The infantile cystinosis levels correspond to those of a 3-mo-old $Ctns^{-/-}$ mouse.

The location of crystals within the stromal keratocytes of $Ctns^{-/-}$ mice is consistent with the histologic findings of patients (3,16,20,22–24). Similarly, corneal crystals have been described as needle shaped or rectangular and smaller than iris crystals. Moreover, corneal vascularization has also been reported (2). In contrast, there are one report of endothelial (3) and one report of epithelial (2) crystals. However, the epithelial location is controversial (3,16,20,23,24), and slit-lamp studies confirmed the stromal (18,19,24) and endothelial (24), but not epithelial, locations.

Although corneal crystals are pathognomic of cystinosis, in one of the youngest (5-wk-old) documented cases, crystals were not detected in the cornea but in the iris (25). This is consistent with the presence of iris and absence of corneal crystals in 1-mo-old $Ctns^{-/-}$ mice and correlates with the

twofold lower corneal cystine levels at this age. Thus, in both patients and *Ctns*$^{-/-}$ mice, iris crystals develop first.

The early appearance (3 mo) of corneal crystals in the mouse model correlates with their early appearance in cystinosis patients, in whom they play a major role in the evolving photophobia. The *Ctns*$^{-/-}$ mice did not show "classic" photophobic behavior (less time in the light box). Paradoxically, they visited the light box more often but for a shorter time than wild-type mice. Such short visits result from an emotional or physical reaction to the brightly lit environment. Because the *Ctns*$^{-/-}$ mice are not more or less anxious than controls (unpublished data), this significant increase of short-duration visits suggests a mild photophobic state.

Retina. Before 19 mo, retinal cystine levels were insufficient for the formation of detectable crystals. Furthermore, the histology of the neural retina and the RPE was normal, consistent with the lack of detectable abnormalities by funduscopic examination (not shown) or in the ERG responses of 22 *Ctns*$^{-/-}$ mice aged 11 mo or younger. We previously reported a decreased ERG response in one (of four studied) 8-mo-old 129Sv-C57BL/6 *Ctns*$^{-/-}$ mouse (9). It could be argued that back-crossing the *Ctns*$^{-/-}$ mice attenuated the ocular phenotype. However, on histologic sections of the 129Sv-C57BL/6 *Ctns*$^{-/-}$ mice, crystals were detected in the choroid and sclera, but rarely in the cornea, and retinal structure was normal. In contrast, we found abundant crystals in many tissues of the C57BL/6 *Ctns*$^{-/-}$ mice, suggesting that the back-crossing amplified the phenotype. Furthermore, the retina is not spared. In the 19- and 22-mo-old mice, we detected rare crystals by TEM in the inner nuclear layer, consistent with the sudden increase in cystine levels. Furthermore, the photoreceptor segments and nuclei were absent and the RPE degenerated.

Similarly, in patients, retinal crystals are rare and occasionally reported in the RPE (3,16), suggesting that they are not a constant disease feature. In contrast, retinal depigmentation is associated early with infantile cystinosis and can precede corneal changes (25). Notably, vacuolization of RPE cells was the only abnormal finding in an 18-wk cystinotic fetus (26). Therefore, the lack of early RPE anomalies in the *Ctns*$^{-/-}$ mice is intriguing. Moreover, as is the case with Fanconi syndrome, the retinopathy is not always associated with the juvenile form and is absent in ocular cystinosis (25). It is tempting to speculate that a common mechanism is rescuing the *Ctns*$^{-/-}$ mice from the Fanconi syndrome and the retinopathy.

Interestingly, the retinopathy in young patients does not cause ocular symptoms (25,27). In contrast, posttransplantation patients whose retinas have accumulated cystine for one to three decades can exhibit an age-dependent decreased visual acuity and/or abnormal ERG profiles (4,27). These findings are consistent with the late appearance of retinal anomalies in the C57BL/6 *Ctns*$^{-/-}$ mice.

Lens. The lens showed the lowest cystine levels consistent with the absence of crystals. Similarly, crystals have not been detected on histologic sections of the lens of cystinosis patients (15,22). There are rare biomicroscopic reports of crystals on the anterior lens surface (4,18,19). However, these may be crystal-laden macrophages that migrated onto a pupillary membrane, thus appearing as refractile deposits on the lens surface (18).

Choroid. In addition to containing abundant crystals, the *Ctns*$^{-/-}$ choroid was the only structure to show early lesions that degenerated with age. The choroid of patients is massively infiltrated with crystals (2,16) and, although degeneration has not been clearly described, less pigment in the periphery choroid of a patient was reported (22). As the choroid is highly vascularized and has an important function in nutrition of the retina, it cannot be ruled out that the retinal anomalies in the *Ctns*$^{-/-}$ mice is a secondary consequence of the choroidal degeneration.

Sclera and optic nerve. The continuity between the sclera and the cornea could explain the concomitant appearance of crystals in these tissues. Furthermore, the sclera of cystinosis patients is the only other tissue containing predominantly needle-shaped crystals (15,16,22). Finally, in sections where the optic nerve was conserved, we detected crystals in the surrounding vascularized tissue (not shown). This is consistent with the crystals reported in the fibrovascular pial septa of the optic nerve, but not in the nerve bundles, of patients (3,15,16).

In summary, the temporospatial pattern of cystine accumulation in the *Ctns*$^{-/-}$ mice closely resembles that of cystinosis patients. This is particularly pertinent in terms of the corneal cystine crystals, which lead to a severe and painful photophobia in patients. Currently, the only treatment is by cysteamine eyedrops, which need to be administered 10–12 times a day (28) and are a considerable constraint. This temporospatial guide of the ocular anomalies of the C57BL/6 *Ctns*$^{-/-}$ mice provides the foundation for testing novel ocular cystine-depleting therapies.

Acknowledgments. The authors thank the IGMM animal house staff for their indispensable help, M. Villain for helpful discussions, C. Depeyre and G. Dubois for technical help, and the Montpellier RIO Imaging platform and CRIC for light and TEM facilities, respectively.

REFERENCES

1. Gahl WA, Thoene J, Schneider J 2001 Cystinosis: A disorder of lysosomal membrane transport. In Scriver CJ, Beaudet AL, Sly WS, Valle D (eds) The Metabolic and Molecular Bases of Inherited Disease. McGraw-Hill, New York, pp 5085–5108
2. Dufier JL, Dhermy P, Gubler MC, Gagnadoux MF, Broyer M 1987 Ocular changes in long-term evolution of infantile cystinosis. Ophthalm Paediatr Genet 8:131–137
3. Gahl WA, Thoene JG, Schneider JA, O'Regan S, Kaiser-Kupfer MI, Kuwabara T 1988 NIH conference. Cystinosis: progress in a prototypic disease. Ann Intern Med 109:557–569
4. Gahl WA, Kaiser-Kupfer MI 1987 Complications of nephropathic cystinosis after renal failure. Pediatr Nephrol 1:260–268
5. Gahl WA, Thoene JG, Schneider J 2002 Cystinosis. N Engl J Med 347:111–121
6. Kalatzis V, Cherqui S, Antignac C, Gasnier B 2001 Cystinosin, the protein defective in cystinosis, is a H(+)-driven lysosomal cystine transporter. EMBO J 20:5940–5949
7. Town M, Jean G, Cherqui S, Attard M, Forestier L, Whitmore SA, Callen DF, Gribouval O, Broyer M, Bates GP, van't Hoff W, Antignac C 1998 A novel gene encoding an integral membrane protein is mutated in nephropathic cystinosis. Nat Genet 18:319–324
8. Kalatzis V, Nevo N, Cherqui S, Gasnier B, Antignac C 2004 Molecular pathogenesis of cystinosis: effect of CTNS mutations on the transport activity and subcellular localization of cystinosin. Hum Mol Genet 13:1361–1371
9. Cherqui S, Sevin C, Hamard G, Kalatzis V, Sich M, Pequignot MO, Gogat K, Abitbol M, Broyer M, Gubler MC, Antignac C 2002 Intralysosomal cystine accumulation in mice lacking cystinosin, the protein defective in cystinosis. Mol Cell Biol 22:7622–7632

10. Smith M, Furlong CE, Greene AA, Schneider JA 1987 Cystine: binding protein assay. Methods Enzymol 143:144–148
11. Reitsamer HA, Kiel JW, Harrison JM, Ransom NL, McKinnon SJ 2004 Tonopen measurement of intraocular pressure in mice. Exp Eye Res 78:799–804
12. Abdeljalil J, Hamid M, Abdel-Mouttalib O, Stephane R, Raymond R, Johan A, Jose S, Pierre C, Serge P 2005 The optomotor response: a robust first-line visual screening method for mice. Vision Res 45:1439–1446
13. Siegel S, Castellan NJ Jr 1988 Nonparametric Statistics for the Behavioral Sciences. McGraw-Hill, New York
14. Savinova OV, Sugiyama F, Martin JE, Tomarev SI, Paigen BJ, Smith RS, John SW 2001 Intraocular pressure in genetically distinct mice: an update and strain survey. BMC Genet 2:12
15. Frazier PD, Wong VG 1968 Cystinosis. Histologic and crystallographic examination of crystals in eye tissues. Arch Ophthalmol 80:87–91
16. Sanderson PO, Kuwabara T, Stark WJ, Wong VG, Collins EM 1974 Cystinosis. A clinical, histopathologic, and ultrastructural study. Arch Ophthalmol 91:270–274
17. Wan WL, Minckler DS, Rao NA 1986 Pupillary-block glaucoma associated with childhood cystinosis. Am J Ophthalmol 101:700–705
18. Kaiser-Kupfer MI, Caruso RC, Minkler DS, Gahl WA 1986 Long-term ocular manifestations in nephropathic cystinosis. Arch Ophthalmol 104:706–711
19. Richler M, Milot J, Quigley M, O'Regan S 1991 Ocular manifestations of nephropathic cystinosis. The French-Canadian experience in a genetically homogeneous population. Arch Ophthalmol 109:359–362
20. Kaiser-Kupfer MI, Chan CC, Rodrigues M, Datiles MB, Gahl WA 1987 Nephropathic cystinosis: immunohistochemical and histopathologic studies of cornea, conjunctiva and iris. Curr Eye Res 6:617–622
21. Harms E, Krauss-Mackiw E, Lutz P 1979 Cystine concentration of cultivated cells from skin and cornea. Metab Pediatr Ophthalmol 3:157–160
22. François J, Hanssens M, Coppieters R, Evens L 1972 Cystinosis. A clinical and histopathologic study. Am J Ophthalmol 73:643–650
23. Kenyon KR, Sensenbrenner JA 1974 Electron microscopy of cornea and conjunctiva in childhood cystinosis. Am J Ophthalmol 78:68–76
24. Melles RB, Schneider JA, Rao NA, Katz B 1987 Spatial and temporal sequence of corneal crystal deposition in nephropathic cystinosis. Am J Ophthalmol 104:598–604
25. Wong VG, Lietman PS, Seegmiller JE 1967 Alterations of pigment epithelium in cystinosis. Arch Ophthalmol 77:361–369
26. Schneider JA, Verroust FM, Kroll WA, Garvin AJ, Horger EO 3rd, Wong VG, Spear GS, Jacobson C, Pellett OL, Becker FL 1974 Prenatal diagnosis of cystinosis. N Engl J Med 290:878–882
27. Yamamoto GK, Schulman JD, Schneider JA, Wong VG 1979 Long-term ocular changes in cystinosis: observations in renal transplant recipients. J Pediatr Ophthalmol Strabismus 16:21–25
28. Kaiser-Kupfer MI, Fujikawa L, Kuwabara T, Jain S, Gahl WA 1987 Removal of corneal crystals by topical cysteamine in nephropathic cystinosis. N Engl J Med 316:775–779